25th ABCM International Congress of Mechanical Engineering
October 20-25, 2019, Uberlândia, MG, Brazil

COB-2019-0166
CHARACTERIZATION AND SIMULATION OF THE DRAPING BEHAVIOUR OF COMPOSITE WOVEN FABRICS

Dante Krivtzoff De' Grandis
Mauricio Vicente Donadon
Alfredo Rocha de Faria
Mariano A. Arbelo
Instituto Tecnológico de Aeronáutica-ITA
dantekdg@hotmail.com; donadon@ita.br; arfaria@ita.br; marbelo@ita.br
Vitor Reis
Alessandro Guimarães
Instituto de Pesquisas Tecnológicas-IPT/Lightweight Structures Laboratory-LEL
vreis@ipt.br; aguimaraes@ipt.br

Abstract. *This work describes an experimental procedure characterization of draping behavior of dry composite woven fabrics using the uniaxial bias extension test. Based on experimental evidence a non-orthogonal hypo-elastic constitutive model that enables tracking of the rotation of fiber during the forming process is proposed and implemented into ABAQUS/Explicit FE code within shell elements. Numerical simulations were performed at the coupon level and subcomponent levels to validate the model. Good agreement between results was found.*

Keywords: *Composite fabrics, draping, finite elements, bias extension test*

1. INTRODUCTION

Processing time is a crucial factor that still limits the application of composites in the aeronautical and automotive industries. Therefore, processes such as thermoforming, or hot-stamping, carried out in a few minutes interval, have attracted attention due to its high pace when compared to other processes in the market (Cao 2014 and Harrison 2013). However, the quality and structural performance of the final component are closely related to the type of material used, tooling/mold and are also dependent on process parameters such as pressure and consolidation temperatures which need to be thoroughly checked before the processes can be fully implemented.

The inherent quality of thermoplastic materials possessing good reparability allied to structural gains in weight and performance when compared to thermoset materials, produce parts that exhibit better maintenance and recyclability characteristics, making these types of material especially advantageous.

The technology and tools used in thermoforming of thermoplastic composite fabrics is similar to that used for metal sheets, but the deformation mechanisms involved during the process are very different, providing greater drapability when compared to their isotropic counterparts (Long 2007). However, the various deformation mechanisms present in this process need a better understanding for the development of robust and practical simulation tools, thus allowing a significant reduction of time and costs associated to the optimal design and fabrication of laminates, tooling and parts. In sheet metal forming the material can be subjected to large membrane deformations, however, in the case of composite material, the membrane deformations are negligible, and the angular variation between the weft and warp fibers, in-plane shear, proves to be the predominant deformation mechanism.

Thermostamping allows for high pace and good reproducibility when compared to other processes in the market. However, the quality and structural performance of the final component are not only closely related to the type of material used and tooling, but are also dependent on process parameters such as pressure and consolidation temperature which need to be thoroughly checked before the processes can be fully implemented.

Among several types of composite materials, thermoplastic woven reinforced ones adapt specially well to the thermostamping process, giving good repeatability in high quality parts. Woven textiles show great distortion characteristics due to the relative movement between warp and weft yarns, and thermoplastic resins possess simpler manufacturing cycles, without a predetermined shelf life and no need to be kept at controlled temperatures. Additionally, they are recyclable and have good reparability characteristics. Nevertheless, there is need for further development of modeling tools and material characterization practices to efficiently implement this manufacturing technique in modern industry.

The yarns ability to slide between each other makes the part`s drapability very expressive, allowing for the production of double curvature complex parts. However, the de-coupling between material rigidities leads to difficulties in characterizing the material macro behavior, whose effects need to be better understood for proper simulation in order to avoid wrinkles and other undesirable defects (Harrison et al., 2004 and Cao et al., 2008).

As of this moment, several modeling strategies of this process have been developed in the literature. Fishnet algorithms comprised the first purely kinematic algorithms whereas more advanced models now include semi-discrete techniques with micro scale mechanics. Among current strategies, continuum mechanics ones can take boundary conditions into account as well as specific drapability related material properties as input with good computational costs. This strategy provides the basis for the development of constitutive models that correctly represent the phenomena involved (Bussetta, P. and Correia, N., 2018). In order to achieve this a non-orthogonal material model based on Aridhi et al. 2017 has been implemented while taking into account the material`s specific in-plane shear behavior. Although the model is a simplified routine that only accounts for the main characteristic influencing the part´s draping, the implemented tool lends itself well in showing possible wrinkle formation zones through the analysis of the conformed textile's shear angles.

2. FABRIC DRAPING CHARACTERIZATION

For small shear angles, the strains are negligible and material global deformation comes from yarn rotation. The stiffness initially comes from friction between the warp and weft yarns. As the angle progresses, lateral contact between yarns start to occur and the subsequent compaction leads to wrinkling (Boisse 2017).

In-plane shear stiffness is the chief parameter defining final shear angles on the formed part as well as the main indicative of wrinkle onset, with in-plane shear being the principal deformation mode for an originally plane part to conform into double curvature geometries. Tests focusing on this parameter not only provide the in-plane shear stiffness, but often the shear locking angle, which is a primary indicative of textile's wrinkling onset. There are mostly two common methods for determining those properties, the bias-extension and the picture frame (trellis-frame) shear tests. The bias extension has the advantage of actually developing a pure shear zone while the standard picture frame apparatus mixes in-plane shear with yarn tensile tension, which can greatly be enhanced if the yarns are not properly aligned with the frame. Since the yarns' tensile stiffness is much higher than the woven material's in-plane shear stiffness the results are greatly affected. Both tests are generally studied together and compared. Also, the experimental rigs of the bias extension are simpler and easier to produce justifying the choice of this test for the current work.
(Boisse et al., 2011, Boisse et al., 2017, Cao et al., 2004, Cao 2008 et al., Cartwright et al., 1999, Gereke et al., 2013, Harrison et al., 2004, Harrison et al., 2012, Launay et al., 2008 and Lebrun et al., 2003).

2.1 Bias Extension Test Setup

A tensile test at 45° on a dry AGP193-P carbon fiber plain weave fabric (known as bias extension shear test) was performed at room temperature to characterize the material`s in-plane shear response, the most dominant deformation mechanism in draping. As can be seen in Figure 1 the test setup is straightforward. A rectangular sample is clamped at two ends and the warp and weft yarns are oriented at 45º to the direction of the applied tensile load. Two pairs of reference lines, perpendicular to each other, were drawn along the warp and weft yarns, as shown in Fig. 1a and Figure 2a (P. Harrison et al. 2012).

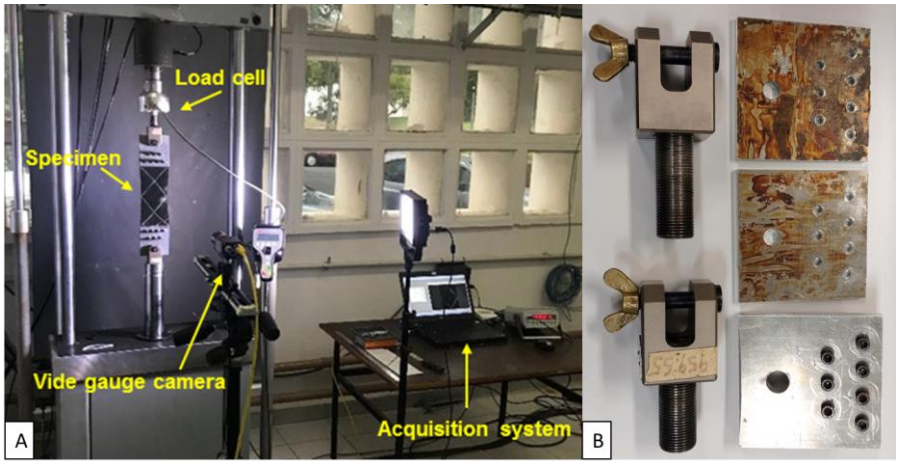

Figure 1 (a) Experimental test setup, (b) Details on the camping system

In Figure 2 different zones of the specimen can be seen. Since region C has both warp and weft yarns clamped, it is assumed it does not distort in shear. Region B has one end clamped and the other one free while region A has both ends clamped. It is assumed ideal shear kinematics in region A, developing pure shear while region B develops half the shear angle developed in region A. As the specimen in this test has three different zones with different kinematics, data analysis is not straightforward. It is assumed that in-plane shear is the dominant energy dissipation mechanism and results are only of interest as long as intertow and intraply slip and out-of-plane bending are not observed. As such, the test is generally carried out to no more than 50º of shear angle and then interrupted (J. Cao et al. 2008).

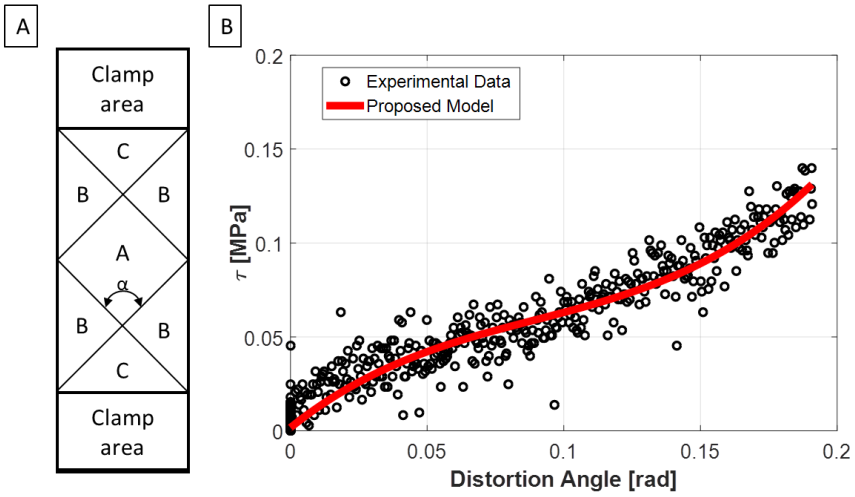

Figure 2 (a) Specimen scheme, (b) Results.

Figure 3 represents the undesired deformation modes. At the far left intertow slip is observed. It is the most dominant mode of deformation at larger shear angles, consisting of the movement of the crossover points between yarns. At the drawing, the black dots represent the current yarn intersection points while the grey ones show the initial undeformed configuration. At item B) intertow slip is observed by a comparison of a non-deformed (left) and a deformed (right) drawing (P. Harrison et al. 2004). In C) the scheme shows basic wrinkle dynamics. At the elliptical center the part deforms out of the plane of the textile, and as a result the edges of the pure shear zone get curved inwards. At D) the author uses this principle to characterize wrinkle onset by performing a length comparison analysis (P. Harrison et al. 2012).

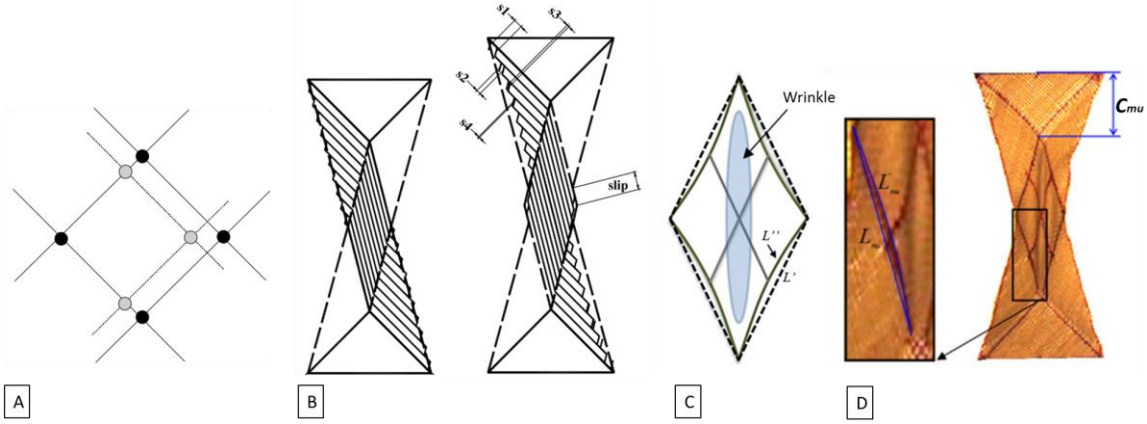

Figure 3 Undesired modes of deformation occurring at higher shear angles in the bias extension test that null further validity of results. The two sketches at left are adapted from P. Harrison 2004 et al. and the other two are adapted from P. Harrison 2012 et al.

2.2 Bias Extension Test Normalization

It is of primary interest that the data obtained is independent of sample size and test technique so that it might be compared to tests like the picture frame or tests where the specimen has different dimensions. To do so, J. Cao et al. (2008) proposed an energy-based procedure. As per Figure 2, the test sample has four different zones with only zones A and B notably contributing to the energy consumption in the test. In an ideal case the work done by the tensile machine is therefore equal to the work absorbed by regions A and B as in the first and second parts of the right hand side of Eq. (1) respectively:

$$F \cdot \dot{\delta} = \left(C_s(\gamma) \cdot A_\gamma \cdot \dot{\gamma}\right) + \left(C_s\left(\frac{\gamma}{2}\right) \cdot A_{\frac{\gamma}{2}} \cdot \frac{\dot{\gamma}}{2}\right) \tag{1}$$

where A_γ is the original area of zone $\frac{A}{2}$, $A_{\frac{\gamma}{2}}$ is the original area of zone B and C_s is the torque needed to deform a unit area of the fabric in shear. The in-plane shear angle γ is defined as:

$$\gamma = \alpha - \frac{\pi}{2} \tag{2}$$

By relating the unit torque to the shear force as in Eq. (3):

$$C_s(\gamma) = F_{sh}(\gamma) \cdot \cos(\gamma) \tag{3}$$

and Eq. (4):

$$C_s\left(\frac{\gamma}{2}\right) = F_{sh}\left(\frac{\gamma}{2}\right) \cdot \cos\left(\frac{\gamma}{2}\right) \tag{4}$$

and using geometrical parameters we arrive at a normalized expression in Eq. (5) for the shear force used on a unit area of textile under pure shear.

$$F_{sh}(\gamma) = \frac{1}{(2H - 3W)\cos\gamma}\left(\left(\frac{H}{W} - 1\right) \cdot F \cdot \left(\cos\frac{\gamma}{2} - \sin\frac{\gamma}{2}\right) - W \cdot F_{sh}\left(\frac{\gamma}{2}\right)\cos\frac{\gamma}{2}\right) \tag{5}$$

Notice that the method gives the shear force incrementally. For further details, refer to J. Cao et al. (2008). The axial displacement and in-plane fabric distortion were acquired with the aid of a Video Gauge system. Figure 1b shows the in-plane shear stress vs. distortion angle obtained experimentally and compares it to predicted results obtained using the proposed model. The distortion angle was measured in respect to the relative rotation between the two initial reference lines, defining a local non-orthogonal coordinate system in the material deformed configuration.

3. NON-ORTHOGONAL HYPOELASTIC CONSTITUTIVE MODEL

The constitutive model formulation presented in this section is based on a previous work proposed by Aridhi et al. (2017). The stress-strain relation at the local ply coordinate system is given as follows,

$$\begin{Bmatrix} \sigma_{11} \\ \sigma_{11} \\ \sigma_{12} \end{Bmatrix} = \begin{bmatrix} C_{11} & C_{12} & 0 \\ C_{12} & C_{22} & 0 \\ 0 & 0 & C_{44} \end{bmatrix} \begin{Bmatrix} \varepsilon_{11} \\ \varepsilon_{22} \\ \gamma_{12} \end{Bmatrix} \rightarrow \boldsymbol{\sigma} = \mathbf{Q}\boldsymbol{\varepsilon} \tag{6}$$

where the stiffness coefficients are represented in Eqs. (7) – (10):

$$C_{11} \rightarrow \begin{cases} \lambda_1 & \text{If } \varepsilon_{11} < 0.0 \\ \dfrac{\lambda_2}{\left(1 + e^{k_1(\varepsilon_{11} - k_2)}\right)} & \text{Otherwise} \end{cases} \tag{7}$$

$$C_{22} \rightarrow \begin{cases} \lambda_3 & \text{If } \varepsilon_{22} < 0.0 \\ \dfrac{\lambda_4}{\left(1 + e^{k_3(\varepsilon_{22} - k_4)}\right)} & \text{Otherwise} \end{cases} \tag{8}$$

$$C_{12} \rightarrow \begin{cases} \lambda_5 C_{11} & \text{If } C_{11} > C_{22} \\ \lambda_5 C_{22} & \text{Otherwise} \end{cases} \tag{9}$$

$$C_{44} = \sum_{i=0}^{4} a_i \cdot \gamma^i \tag{10}$$

The material constants λ_i, k_i and a_i are related to the fabric drapability behavior, obtained from uniaxial tensile tests with the fabric yarns aligned 0º, 90º and 45º from the loading direction (bias extension test) and γ is the current shear angle of the fabric updated at each time step (its definition is seen in Eq. 2). ε_{11} and ε_{22} are the strains in the warp and weft directions respectively.

A complexity of modelling composites' drapability comes from the high in-plane distortions that induce variations in the angle between the warp and weft yarns, changing the values of mechanical material properties. The second problem is that the material reference frame will be different from the element frame. Therefore, the update of anisotropic material properties is necessary in the material definition in the finite element analysis (FEA) of draping problems. As such, the updated material behavior law needs to be formulated on the basis of changing directions of the unidirectional fibre laminates corresponding to the warp and weft directions of the woven fabric. The woven fabrics with warp and weft yarns are treated as two-ply unidirectional laminates: one ply comprising fibres in the warp and the other representing the fibres in the weft direction. This laminate is initially oriented as [0°/90°] in an (M_1, M_2) global coordinate system (see Fig. 4). It becomes [(γ/2), (γ/2+α)] in the ($\mathbf{n_p}$, $\mathbf{n_t}$) local material coordinates which are rotated with the material points during deformation. This results in the local orientation of fibres varying at each material point and at each time increment of the simulation.

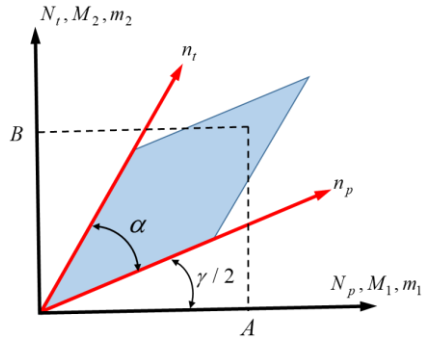

Figure 4 Pure shear deformation of woven fabric – adapted from Dong et al (2001).

The material frame directions $\boldsymbol{m}_1$ and $\boldsymbol{m}_2$ are related to the material global coordinate system $\mathbf{M}_1$ and $\mathbf{M}_2$ through the following coordinate transformation,

$$\mathbf{m_1} = \mathbf{R}.\mathbf{M_1} \tag{11}$$

$$\mathbf{m_2} = \mathbf{R}.\mathbf{M_2} \tag{12}$$

$\mathbf{R}$ is obtained from the deformation gradient tensor $\mathbf{F}$ by using the polar decomposition theorem given as follows. $\mathbf{U}$ is defined as a right stretch tensor, and the directions $\boldsymbol{n}_p$ and $\boldsymbol{n}_t$ are described by the product of $\mathbf{F}$ by $\mathbf{N_P}$ and $\mathbf{N_t}$ respectively as in Eq. (14) and Eq. (15). $\mathbf{N_P}$ and $\mathbf{N_t}$ are unit vectors that describe the warp and weft directions of the fabric in the initial configuration (since fibres are initially oriented at 0º/90º, $\mathbf{N_P}$ and $\mathbf{N_t}$ have the same directions as $\mathbf{M}_1$ and $\mathbf{M}_2$):

$$\mathbf{F} = \mathbf{R}.\mathbf{U} \tag{13}$$

$$\mathbf{n_p} = \mathbf{F}.\mathbf{N_p} \tag{14}$$

$$\mathbf{n_t} = \mathbf{F}.\mathbf{N_t} \tag{15}$$

The angle between the warp and weft directions in the deformed configuration can then be evaluated as,

$$\alpha = \cos^{-1}\left(\frac{\mathbf{n_p}.\mathbf{n_t}}{|\mathbf{n_p}||\mathbf{n_t}|}\right) \tag{16}$$

while the previously defined shear angle follows the relation:

$$\frac{\gamma}{2} = \cos^{-1}\left(\frac{\mathbf{n_p}.\mathbf{m_1}}{|\mathbf{n_p}||\mathbf{m_1}|}\right) \tag{17}$$

The stiffness matrix in the off-axis coordinates system (***x***, ***y***) can then be obtained by a matrix transformation using the following relation,

$$\bar{\mathbf{Q}} = \mathbf{T}(\theta)^{-1}\mathbf{Q}\mathbf{T}(\theta) \tag{18}$$

where **T** is the transformation matrix that relates local-to-global coordinate material systems, given as follows.

$$\mathbf{T}(\theta) = \begin{bmatrix} c^2\theta & s^2\theta & 2c\theta s\theta \\ s^2\theta & c^2\theta & -2c\theta s\theta \\ -c\theta s\theta & c\theta s\theta & c^2\theta - s^2\theta \end{bmatrix} \tag{19}$$

Finally, in Eq. (20) the updated material behavior law is derived by simply adding tensor $\bar{\mathbf{Q}}^p$ expressing the warp unidirectional laminate at an angle $\gamma/2$ in respect to the off-axis coordinates system (***m*₁, *m*₂**) to tensor $\bar{\mathbf{Q}}^t$ expressing the weft unidirectional laminate at an angle $\alpha + \gamma/2$. The updated stresses are given by Eq.(21), where **σ** and **ε** are the updated stresses and strains respectively.

$$\tilde{Q}_{ij} = \bar{Q}^p_{ij}(\gamma/2) + \bar{Q}^t_{ij}(\alpha + \gamma/2) \tag{20}$$

$$\boldsymbol{\sigma} = \tilde{\mathbf{Q}}\boldsymbol{\varepsilon} \tag{21}$$

3.1 Prediction of fibre volume fraction variation

If matched-die moulding tools are used, the thickness *t* of the component is constant and the fibre volume fraction, v_f, is variable. For pure shear deformation, the amount of material in a small initially square element would remain the same after shear deformation and it is possible to show that the ratio of the volume fraction after and before deformation, neglecting fabric thickness variation, is:

$$v_f^0 \times a \times b \times t_0 = v_f^f \times a \times b \times t \times \sin\alpha \quad ; \tag{22}$$

Since *t* equals t_0 we have:

$$\frac{v_f^f}{v_f^0} = \frac{1}{\sin\alpha} \tag{23}$$

where the distribution of the local element angle α in the composite product can be determined from the simulation.

4. FABRIC DRAPING SIMULATION

The proposed constitutive model has been implemented into ABAQUS/Explicit Finite Element Code within S4R shell elements, a general-purpose reduced integration linear 4 sided shell element with four nodes and six degrees of freedom per node. Simulations at coupon and subcomponent levels were performed in order to check the model capability to predict the behavior of the woven fabric studied herein. Figure 5a compares the morphologies of the predicted distortion with those experimentally observed during the bias extension shear test at room temperature carried out at ITA for AGP193-P dry carbon woven fabrics, provided by Hexcel. Figure 5b is the comparison of predicted spherical hat profile of a draped fabric with experimental results and a similar model available in the open literature for glass fibre woven fabric (Dong et al., 2001). Figure 5c is the result obtained by the current analysis for the same conditions, where a similar result was obtained.

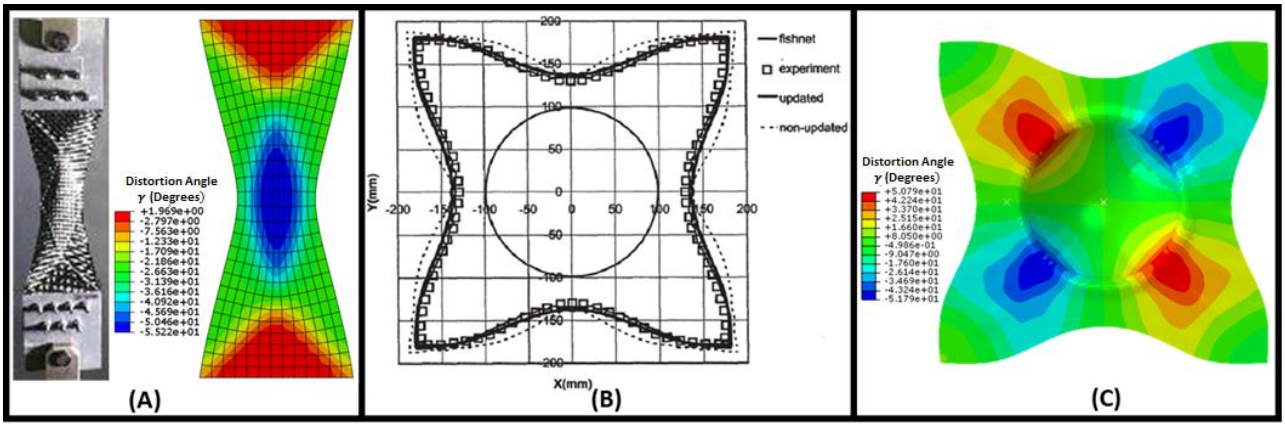

Figure 5 (A) Comparison between predicted and experimental distortions observed in the bias extension test, (B) Experimental and Numerical results by Dong et al. (1999) and (C) predicted profiles of draped fabric.

Figure 6 shows a simulation of a classical benchmark available in the literature including a rigid punch, a die, a holder and the woven fabric blank. The model of a hemispherical hat shape with a flat rim was selected to match the experimental set-up commonly used for draping validations. The punch is a hemispherical male mould with a radius of 98.6 mm joined with a cylindrical flange at the upper end. The die is a spherical hat shape female mould with a radius of 100.4mm in the hemisphere and a radius of 240 mm in the flat disc part. The holder is a flat plate disk to hold the fabric in draping. The blank material is a glass woven fabric of thickness of 0.64 mm representing an 8 harness satin dry glass woven fabric. An overall good correlation between experimental and numerical results was obtained in both coupon and sub-component levels, where errors less than 10% were found between measured (Dong et al., 2001) and predicted in-plane shear distortions. Item (A) shows the initial model, item (B) predicted in-plane shear distortions and (C) final fibre volume fraction distribution on the part.

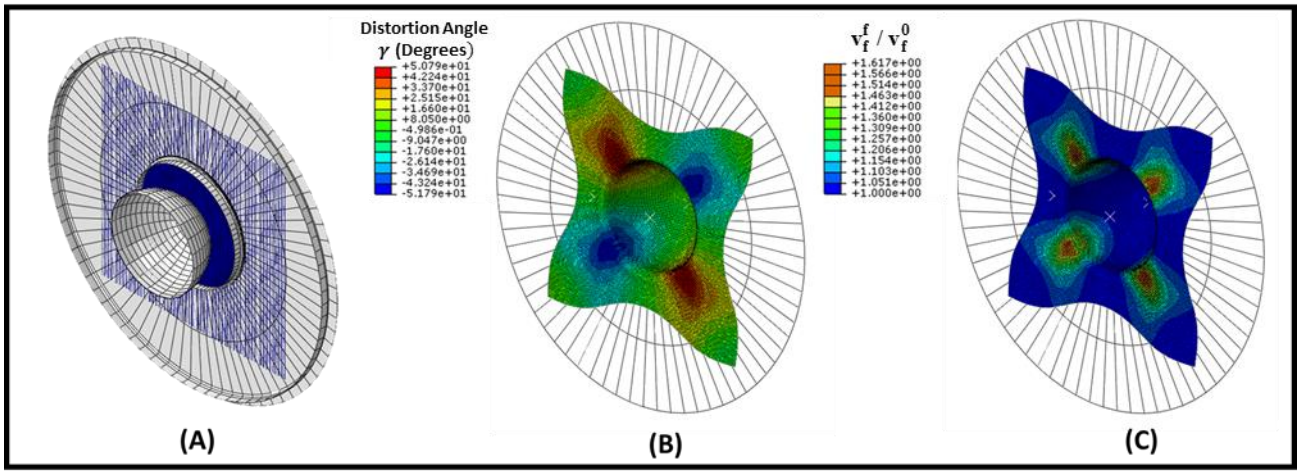

Figure 6. (a) Details on the FE model for the rigid punch, a die, a holder and the woven fabric blank, (b) Predicted distortions, (c) Predicted variations in the fiber volume fraction v_f^f / v_f^0

5. CONCLUSION

A composite`s drapability is defined by the conjunction of many factors. The tensile, in-plane shear and out-of-plane bending stiffnesses, the frictional behavior between layers and the composite and the tooling and the coupling between those responses as well as its dependence on temperature. Nevertheless, as long as the main mechanisms are taken into account, good results can be achieved with fair simplicity. As shown in this work, in plane shear distortions define the main deformation mechanism observed in thin dry woven fabric laminates, and the obtained material shear angles after deformation can give an indication of possible wrinkle initiation zones.

The next step would comprise more relevant and easy to obtain material characteristics, such as out-of-plane bending behavior so as to enable the modeling of wrinkle shape, a needed information to observe if wrinkle would extend to the useful part of the preform. The interdependence between material behaviors for different modes can be obtained either experimentally of through meso-scale analysis and then implemented on the macro-scale model (Boisse et al., 2011, Bussetta, P. and Correia, N., 2018 and Harrison et al. 2012).

A good correlation between the numerical simulations and experimental results in both coupon and sub-component levels was obtained using the proposed modeling methodology, but the simplifications used limit its use to reasonably simple geometries and only predict the obtained material shear angle, without inferring on possible wrinkle shapes. The model will be further extended to handle complex thick semi-preg based thermoplastic laminates where temperature, pressure consolidation and ply friction effects will be taken into account in the formulation.

The results presented herein are part of the *São Paulo Initiative on Research on Innovative Thermoplastic Composites Solutions* (SPIRIT) consortium, which was formed in 2017 as a joint initiative between TenCate Advanced Composites and key aerospace suppliers and educational institutes across Brazil, to collaborate and develop a regional knowledge-base in thermoplastic composite technology for the next generation of aircraft. Partners include Embraer, Alltec, Technological Institute of Aeronautics (ITA), Instituto de Aeronáutica e Espaço (IAE), São Paulo State University (UNESP) and the Institute for Technological Research of the State of São Paulo (IPT).

6. REFERENCES

Aridhi, A., Mabrouki, T., Arfaoui, M., Naouar, N., Boisse, P. and Zarroug, M, 2017. “Modeling and numerical simulation of the drawing of a dry woven reinforcement : Sensitivity of the shear angle to the parameters of the process”. In *Proceedings of the 23ème Congrès Français Mécanique*, Lille, France.

Boisse, P., Hamila, N., Guzman-Maldonado, E., Madeo, A., Hivet, G., dell’Isola, F., 2017. “The bias-extension test for the analysis of in-plane shear properties of textile composite reinforcements and prepregs: a review”. International Journal of Material Forming, Vol. 10, No. 4, pp. 473–492.

Boisse, P., Hamila, N., Vidal-Sallé, E., & Dumont, F., 2011. “Simulation of wrinkling during textile composite reinforcement forming. Influence of tensile, in-plane shear and bending stiffnesses”. Composites Science and Technology, Vol. 71, Issue 5, pp. 683–692.

Bussetta, P.and Correia, N., 2018. "Numerical forming of continuous fibre reinforced composite material: A review". Composites Part A: Applied Science and Manufacturing., Vol. 113, pp. 12–31.

Cao, J., Akkerman, R.; Boisse, P.; Chen, J. and Cheng, H. S. et al., 2008. "Characterization of mechanical behavior of woven fabrics: Experimental methods and benchmark results". Composites Part A: Applied Science and Manufacturing., Vol. 39, No. 6, pp. 1037–1053.

Cao, J., Cheng, H., Yu, T., Zhu, B., Tao, X.; Lomov, S.; Stoilova, T.;Verpoest, I.; Boisse, P.; Launay, J.; Others, 2004 “A cooperative benchmark effort on testing of woven composites”. In *Proceeding of the 7th int. ESAFORM conference on material forming*, Trondheim, Norway, Vol.20, pp.305-8.

Cartwright, B., de Luca, P., Wang, J., Stellbrink, K., & Paton, R., 1999. “Some proposed experimental tests for use in finite element simulation of composite forming”. In *12th International Conference on Composite Materials (ICCM-12)*. Paris, France.

Dong, L., Lekakou, C., Bader, M.G., 2001. “Processing of Composites: Simulations of the Draping of Fabrics with Updated Material Law, Journal of Composite Materials”, Vol. 35, pp. 138-163.

Gereke, T., Döbrich, O., Hübner, M., & Cherif, C., 2013. “Experimental and computational composite textile reinforcement forming: A review”. Composites Part A: Applied Science and Manufacturing, Vol. 46, No. 1, pp. 1-10.

Harrison, P., Abdiwi, F., Guo, Z., Potluri, P., Yu, W. R., 2012. “Characterising the shear–tension coupling and wrinkling behaviour of woven engineering fabrics”. Composites Part A: Applied Science and Manufacturing., Vol. 43, No. 6, pp. 903–914.

Harrison, P., Clifford, M. J. and Long, A. C., 2004. "Shear characterisation of viscous woven textile composites: A comparison between picture frame and bias extension experiments". Composites Science and Technology., Vol. 64, No. 10 - 11, pp. 1453–1465.

Harrison, P.; Gomes, R.; Curado-Correia, N. 2013. “Press forming a 0/90 cross-plyadvanced thermoplastic composite using the double-dome benchmark geometry”. Composites Part A: Applied Science and Manufacturing, Vol. 54, pp.56–69.

Launay, J., Hivet, G., Duong, A. V., & Boisse, P., 2008. “Experimental analysis of the influence of tensions on in plane shear behaviour of woven composite reinforcements”. Composites Science and Technology, Vol. 68, Issue 2, pp. 506–515.

Lebrun, G., Bureau, M. N., & Denault, J., 2003. “Evaluation of bias-extension and picture-frame test methods for the measurement of intraply shear properties of PP/glass commingled fabrics”. Composite Structures, Vol. 61, Issue 4, pp. 341–352.

Long, A. C. A. C.; 2007. *Composites forming technologies.* Woodhead Publishing Limited and The Textile Institute Woodhead Publishing Limited, Abington Hall, ISBN 9781845692537.

7. RESPONSIBILITY NOTICE

The authors are the only responsible for the printed material included in this paper.